Excitonic absorption in gate controlled graphene quantum dots

A. D. Güçlü,[1] P. Potasz,[1,2] and P. Hawrylak[1]

[1]*Institute for Microstructural Sciences, National Research Council of Canada , Ottawa, Canada*
[2]*Institute of Physics, Wroclaw University of Technology, Wroclaw, Poland*

(Dated: July 22, 2010)

We present a theory of excitonic processes in gate controlled graphene quantum dots. The dependence of the energy gap on shape, size and edge for graphene quantum dots with up to a million atoms is predicted. Using a combination of tight-binding, Hartree-Fock and configuration interaction methods, we show that triangular graphene quantum dots with zigzag edges exhibit optical transitions simultaneously in the THz, visible and UV spectral ranges, determined by strong electron-electron and excitonic interactions. The relationship between optical properties and finite magnetic moment and charge density controlled by an external gate is predicted.

Two-dimensional graphene monolayer exhibits fascinating electronic [1–6] and optical properties[7–15] due to the zero energy gap and relativistic-like nature of quasiparticle dispersion close to the Fermi level. With recent improvements in nanofabrication techniques[16] the zero energy gap of bulk graphene can be opened via engineering size, shape, character of the edge and carrier density, and this in turn offers possibilities to simultaneously control electronic[17–25], magnetic[16, 23–30] and optical[30–32] properties of a single-material nanostructure.

In this paper, we present a theory and results of numerical calculations predicting the dependence of the energy gap on shape, size and edge for graphene quantum dots with up to a million atoms. We show that triangular graphene quantum dots with zigzag edges combine magnetic and optical properties tunable with carrier density, with optical transitions simultaneously in the THz, visible and UV spectral ranges. We describe one electron properties of graphene quantum dots with N atoms and N_e π_z electrons by a combination of tight-binding approach with a self-consistent Hartree-Fock method (TB-HF) described in detail in the EPAPS document of our earlier work Ref.(26). Then, in order to take into account correlation and excitonic effects, we solve the many-body Hamiltonian given by

$$\begin{aligned} H &= \sum_{p',\sigma} \epsilon_{p'} b^\dagger_{p'\sigma} b_{p'\sigma} + \sum_{p,\sigma} \epsilon_p h^\dagger_{p\sigma} h_{p\sigma} \\ &+ \frac{1}{2} \sum_{\substack{p'q'r's' \\ \sigma\sigma'}} \langle p'q'|V_{ee}|r's'\rangle b^\dagger_{p'\sigma} b^\dagger_{q'\sigma'} b_{r'\sigma'} b_{s'\sigma} \\ &+ \frac{1}{2} \sum_{\substack{pqrs \\ \sigma\sigma'}} \langle pq|V_{ee}|rs\rangle h^\dagger_{p'\sigma} h^\dagger_{q'\sigma'} h_{r'\sigma'} h_{s'\sigma} \\ &+ \sum_{\substack{p'qrs' \\ \sigma\sigma'}} (\langle rp'|V_{ee}|s'q\rangle - \delta_{\sigma\bar{\sigma}'} \langle rp'|V_{ee}|qs'\rangle) b^\dagger_{p'\sigma} h^\dagger_{q\sigma'} h_{r\sigma'} b_{s'\sigma} \end{aligned} \quad (1)$$

where $b^\dagger_{p'\sigma}$ and $h^\dagger_{p\sigma}$ are hole and electron creation operators corresponding to TB-HF quasi-particles. Excitonic

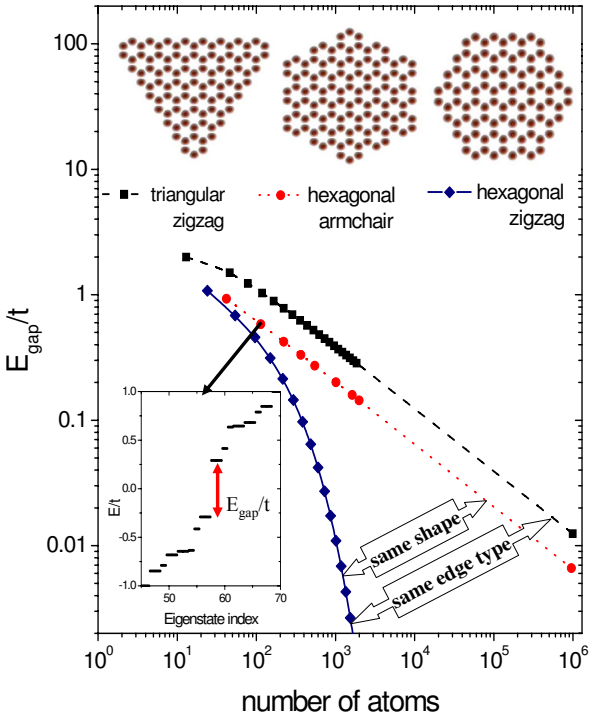

FIG. 1: (Color online) Tight-binding bandgap energy as a function of total number of atoms N for a triangular zigzag quantum dot (black squares), hexagonal armchair quantum dot (red circles), and hexagonal zigzag quantum dot (blue diamonds). The inset shows the tight-binding energy spectrum in the vicinity of the Fermi level for the hexagonal armchair dot.

absorption spectrum between ground state $|\nu_G\rangle$ and excited states $|\nu_f\rangle$ can then be calculated using

$$A(\omega) = \sum_f |\langle \nu_G|P|\nu_f\rangle| \delta(\omega - [E_f - E_G])) \quad (2)$$

where $P = \sum_{pp'} \delta_{\sigma\bar{\sigma}'} \langle p|\mathbf{r}|p'\rangle h_{p\sigma} b_{p'\sigma'}$ is the polarization operator.

The electronic properties of graphene quantum dots depend on the size, shape and the character of the edge.

This is illustrated by comparing electronic properties of three graphene quantum dots including (i) hexagonal dot with armchair edges, (ii) hexagonal dot with zigzag edges, and (iii) triangular dot with zigzag edges (see the inset of Fig. 1). The electronic structures are computed using tight-binding Hamiltonian only with nearest-neighbor hopping for different number of atoms N. An example of the energy levels for $N = 98$ hexagonal quantum dot with armchair edges is shown in the inset of Fig. 1. The red arrow indicates the bandgap separating the occupied valence band states from the empty conduction band states. The dependence of the gap on the number of atoms is plotted in Fig.1. For the hexagonal dot (red circles), the gap decays as the inverse of the square root of number of atoms N, from hundred to million atom nanostructures. This is expected for confined Dirac fermions with photon-like linear energy dispersion ($E_{gap} \propto k_{min} \approx 2\pi/\Delta x \propto 1/\sqrt{N}$), as pointed out in Refs.(23, 31, 33). However, the replacement of the edge from hexagonal to the zigzag has a significant effect on the energy gap. The energy gap of hexagonal structure with zigzag edges decreases rapidly as the number of atoms increases. This is due to the zigzag edges leading to localized states at the edge of the quantum dot, similar to whispering gallery modes of photons localized at the edge of photonic microdisk[34]. Fig. 1 also shows the effect on the energy gap of deforming the hexagonal structure into a triangle while keeping zigzag edges. The energy gap of a triangular dot is extracted from the energy spectrum, an example of which is shown in Fig. 2(a) for a triangular quantum dot with N=96. In addition to valence and conduction bands, the spectrum shows a shell of degenerate levels at the Fermi level [23, 25–30]. The energy gap shown in Fig. 1 corresponds to transitions from the topmost valence to the lowest conduction band state (see Fig. 2(a). Despite the presence of the zero energy shell, the energy gap in the triangular zigzag structure follows the power law $E_{gap} \propto \sqrt{N}$. We note that the energy gap changes from ≈ 2.5 eV (green light) for a quantum dot with ≈ 100 atoms to ≈ 30 meV (8 THz) for a quantum dot with a million atoms and a diameter of ≈ 100 nm. The presence of a partially occupied band of degenerate states in the middle of a well defined energy gap offers unique opportunity to simultaneously control magnetic and optical properties of triangular graphene nanostructures. Indeed, due to the presence of the zero-energy band in the middle of the energy gap, several different photon energies corresponding to transitions within the zero-energy band, into and out of the zero-energy states, and valence-to-conduction band states are possible. This offers interesting possibilities for opto-electronic, opto-spintronic and intermediate-band solar cell photo-voltaic applications [32, 35].

The dependence of optical and magnetic properties on the filling of the shell of degenerate zero-energy states is investigated in detail for a small triangular dot with

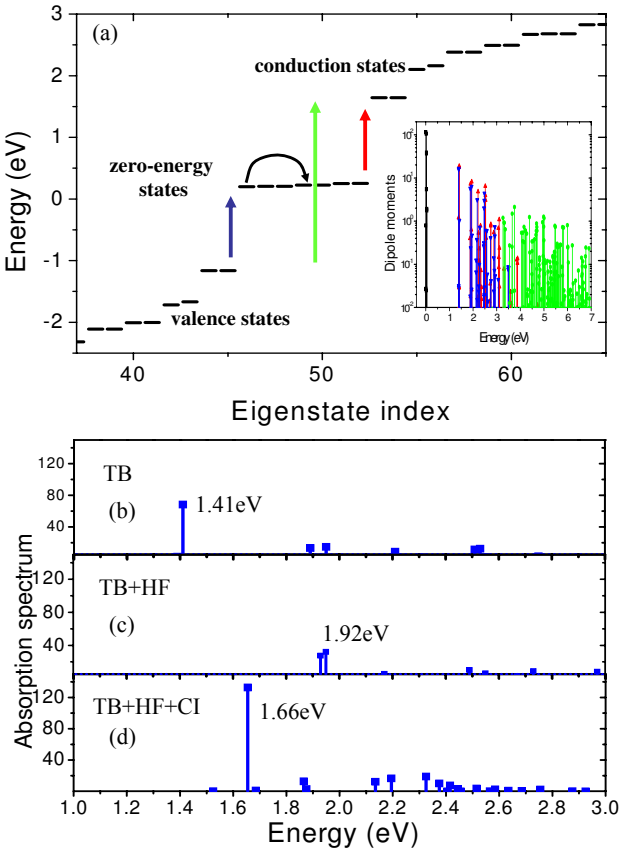

FIG. 2: (Color online) (a) Single particle tight-binding energies of states near Fermi level for a N=96-atom triangular zigzag quantum dot. The colored arrows represent optical transitions from valence to conduction band (VC, green), valence to zero-energy band (VZ, blue), zero-energy to conduction band (ZC, red) and zero-energy to zero-energy band (ZZ, black). Inset shows corresponding dipole moments for all transitions up to 7 eV, obtained using tight-binding orbitals. Figs. (b-d) shows the effect of electron-electron interactions on the VZ transitions within (c) Hartree-Fock approximation, and including (d) correlations and excitonic effect obtained from exact configuration interaction calculations.

zigzag edges containing N=96 atoms. For this system size, exact many-body calculations can be carried out. The degenerate band in the energy spectrum, shown in Fig. 2(a), has $N_z = 7$ zero-energy states. Each state is singly occupied and all electrons have parallel spin [26–29]. We can thus classify allowed optical transitions into four classes, as shown in Fig. 2(a): (i) from valence band to zero-energy degenerate band (VZ transitions, blue color); (ii) from zero-energy band to conduction band (ZC transitions, red color); (iii) from valence band to conduction band (VC transitions, green color); and finally, (iv) within zero-energy states (ZZ transitions, black color). As a consequence, there are three different photon energy scales involved in the absorption spectrum. The corresponding joint optical density of states,

calculated using dipole moments $|\langle i|\mathbf{r}|f\rangle|^2$ connecting initial and final states with energies E_is and E_fs, are shown in the inset of Fig. 2(a). VC transitions (green) occur above full bandgap (≈ 2.8 eV), VZ (blue) and ZC (red) transitions occur starting at half bandgap (≈ 1.4 eV), and ZZ (black) transitions occur at THz energies. The energies corresponding to ZZ transitions are controlled by the second nearest-neighbor tunneling matrix element t_2 and by electron-electron interactions.

Fig. 2(b-d) illustrates in detail the effect of electron-electron and final-state (excitonic) interactions on the absorption spectra. Fig. 2(b) shows detailed VZ absorption spectrum for noninteracting electrons. This spectrum corresponds to transitions from the filled valence band to half filled shell of $N_z = 7$ zero-energy states. Half-filling implies that each state of the zero-energy band is optically allowed. Numerical and analytical calculations show that among the $N_z = 7$ zero-energy states there are two bulk like states, which couple strongly to the valence band resulting in the main transition at $E = 1.41$ eV. The remaining peaks in the absorption spectrum reflect transitions from the discrete spectrum of the valence band. When the electron-electron interactions are turned on, the ground state becomes a Slater determinant of self-consistently calculated Hartree-Fock orbitals: Valence states are doubly occupied, and zero-energy states are singly occupied by an electron with the same spin, e.g., down. The photon energies corresponding to optical transitions $\omega = (E_f + \Sigma_f) - (E_i + \Sigma_i)$ are renormalized by the difference in quasi-particle self-energies $\Sigma_f - \Sigma_i$. The absorption spectrum, shown in Fig. 2(c), is renormalized with transition energies blue-shifted by 0.51 eV to $E = 1.92$ eV. Finally, when final state interactions between all interacting quasi-electron and quasi-hole states are taken into account, the excitonic spectrum is again renormalized from the quasi-particle spectrum, with transitions red shifted from quasi-particle transitions at $E = 1.92$ eV, down to $E = 1.66$ eV. As we can see, electron-electron interactions play an important role in determining energies and form of the absorption spectrum, with net blue shift from the noninteracting spectrum by 0.25 eV.

We now turn to the analysis of the effect of carrier density on the optical properties of graphene quantum dots. The finite carrier density, controlled by either metallic gate or via doping (intercalation), has been shown to significantly modify optical properties of graphene [7, 8, 11, 12]. For a quantum dot, the metallic gate shown in Fig. 3(a), changes the number of electrons in the degenerate shell from N_z to $N_z + \Delta N_z$. This is illustrated in Fig. 3(b) where 4 electrons were removed and 3 electrons remain. These remaining electrons populate degenerate shell and their properties are entirely controlled by their interaction. Alternatively, removal of electrons from charge neutral shell corresponds to addition of holes. As is clear from Fig. 3(b), such a removal of electrons allows

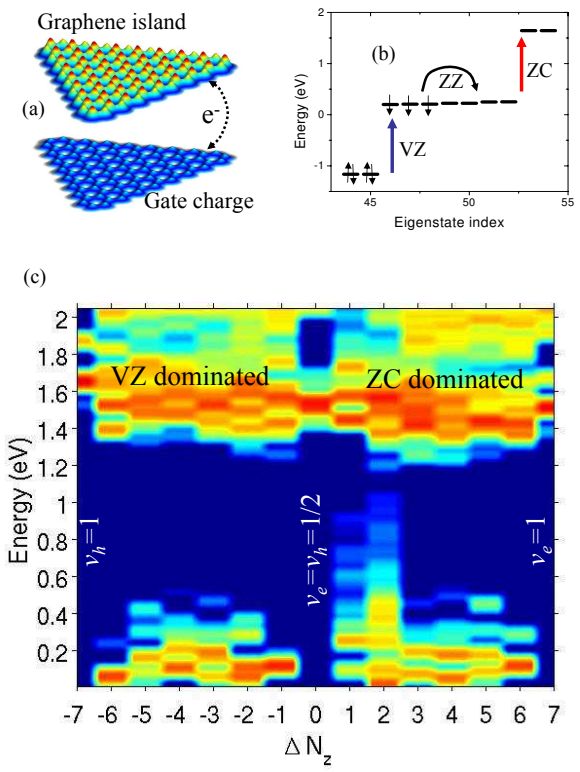

FIG. 3: (Color online) (a) Schematic representation of a TGQD with $N = 97$ carbon atoms with 4 electrons moved to the metallic gate. (b) Corresponding single particle tight-binding configuration near the Fermi level. (c) Excitonic absorption spectrum as a function of energy and charging ΔN_z. For convenience, transitions are artificially broadened by 0.02 eV. Peaks below 0.6 eV are due to ZZ transitions, peaks above 1.2 eV are due to VZ (mostly on the left), and ZC (mostly on the right) transitions. Charge neutral case corresponds to $\Delta N_z = 0$ (filling factors $\nu_e = \nu_h = 1/2$). At $\Delta N_z = 7$, the degenerate band of zero states is completely filled with electrons ($\nu_e = 1$).

intra-shell transitions ZZ, enhances VZ transitions by increasing the number of allowed final states and weakens the ZC transitions by decreasing the number of occupied initial states. Fig. 3(c) illustrates the overall effects in the computed excitonic absorption spectra for VZ, ZC, and ZZ transitions as a function of the number of additional electrons ΔN_z, related to shell filling and/or gate voltage. At $\Delta N_z = -7$ (hole filling factor $\nu_h = 1$), the shell is empty and VZ transitions describe an exciton built of a hole in the valence band and an electron in the degenerate shell. The absorption spectrum has been described in Fig. 2(b-d) and is composed of one main excitonic peak at 1.66 eV. There are no ZC transitions and no ZZ transitions in the THz range. When we populate the shell with electrons, the VZ excitonic transition turns into a band of red shifted transitions corresponding to an exciton interacting with additional electrons, in analogy

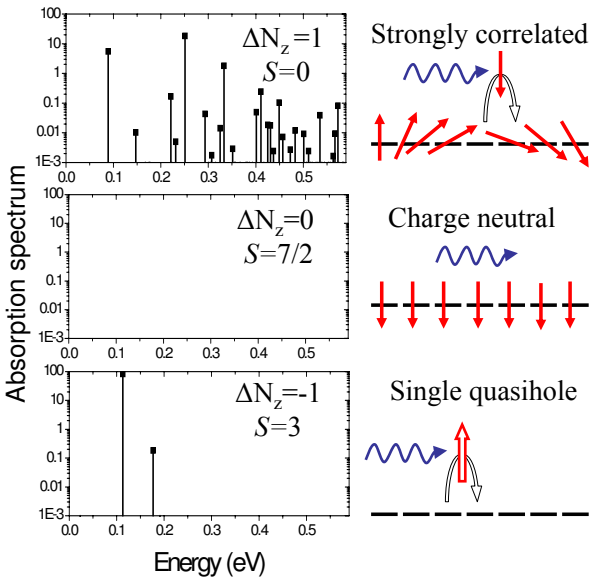

FIG. 4: (Color online) Excitonic absorption spectrum at ΔN_z =-1, 0, and 1 (on the left). Corresponding ground state spins are $S = 3$ (fully polarized), $S = 7/2$ (fully polarized), and $S = 0$ (completely depolarized), respectively. The physics involved in optical transitions is schematically represented on the right side.

to optical processes in the fractional quantum Hall effect and charged semiconductor quantum dots[36]. As the shell filling increases, the number of available states decreases and the VZ transitions are quenched while ZC and ZZ transitions are enhanced. These results show that the absorption spectrum can be tuned by shell filling, which can be experimentally controlled by applying a gate voltage. This is particularly true for the ZZ transitions in the THz range, which can be turned off by either emptying/filling the shell $\Delta N_z = \pm 7$ or at half-filling. At half-filling, electron exchange leads to spin polarization, with each state of the shell filled by a spin polarized electron. Since photons do not flip electron spin, no intra-shell transitions are allowed and the magnetic moment of graphene quantum dot is directly reflected in the ZZ absorption spectrum. In addition, it was shown that even though at charge neutrality ($\Delta N_z = 0$) the system is fully spin polarized, addition (but not subtraction) of a single electron leads to full spin depolarization[26]. This correlation effect plays an important role in the optical transitions involving zero energy states, shown in Fig. 3(c) for $\Delta N_z = \pm 1$.

In Fig. 4, we study the transitions for $\Delta N_z = 0, \pm 1$ in detail. Fig. 4(b) shows the lack of absorption for half-filled spin polarized shell. The right hand side illustrates the fact that photons pass through since they are not able to induce electronic transitions and be absorbed. For $\Delta N_z = -1$, Fig. 4(c), one electron is removed creating a hole in the spin polarized shell. Thus, the absorption spectrum corresponds to transitions from ground state to optically allowed excited states of the hole. The absorption spectrum for an additional electron, $\Delta N_z = +1$, shown in Fig. 4(a), is dramatically different. The additional electron depolarizes the spins of all electrons present, with total spin of the ground state $S = 0$[26]. The strongly correlated ground state has many configurations, which effectively allow for many transitions of the spin up and spin down electrons, as seen in Fig. 4(a). This asymmetry in the THz absorption spectra allows for the optical detection of charge of the quantum dot and correlated electron states in the degenerate electronic shell.

Acknowledgement. The authors thank M. Korkusinski, O. Voznyy, A. Wojs and M. Potemski for discussions and NRC-CNRS CRP, Canadian Institute for Advanced Research, Institute for Microstructural Sciences, and QuantumWorks for support.

[1] P. R. Wallace, Phys. Rev. **71** , 622 (1947).
[2] K. S. Novoselov, A. K. Geim, S. V. Morozov, D. Jiang, Y. Zhang, S. V. Dubonos, I. V. Grigorieva, and A. A. Firsov, Science **306**, 666 (2004).
[3] K. S. Novoselov, A. K. Geim, S. V. Morozov, D. Jiang, M. I. Katsnelson, I. V. Grigorieva, S. V. Dubonos, and A. A. Firsov, Nature **438**, 197 (2005).
[4] Y. B. Zhang, Y. W. Tan, H. L. Stormer, and P. Kim, Nature **438**, 201 (2005).
[5] S. Y. Zhou, G. H. Gweon, J. Graf, A. V. Fedorov, C. D. Spataru, R. D. Diehl, Y. Kopelevich, D. H. Lee, S. G. Louie, and A. Lanzara, Nature Phys. **2**, 595 (2006).
[6] A. H. C. Neto, F. Guinea, N. M. R. Peres, K. S. Novoselov, and A. K. Geim, Rev. of Mod. Phys. **81**, 109 (2009).
[7] D. M. Hoffman, P. C. Eklund, R. E. Heinz, P. Hawrylak, K. R. Subbaswamy, Phys. Rev. B **31** , 3973 (1985).
[8] J. Blinowski, N. H. Hau, C. Rigaux, J. P. Vieren, R. Le Toullec, G. Furdin, A. Herold, J. Melin, J. Physique **41** , 47 (1980).
[9] M. L. Sadowski, G. Martinez, M. Potemski, C. Berger, and W. A. de Heer, Physical Review Letters **97** (2006).
[10] R. R. Nair, P. Blake, A. N. Grigorenko, K. S. Novoselov, T. J. Booth, T. Stauber, N. M. R. Peres, and A. K. Geim, Science **320**, 1308 (2008).
[11] F. Wang, Y. B. Zhang, C. S. Tian, C. Girit, A. Zettl, M. Crommie, and Y. R. Shen, Science **320**, 206 (2008).
[12] Z. Q. Li, E. A. Henriksen, Z. Jiang, Z. Hao, M. C. Martin, P. Kim, H. L. Stormer, and D. N. Basov, Nature Physics **4**, 532 (2008).
[13] K. F. Mak, M. Y. Sfeir, Y. Wu, C. H. Lui, J. A. Misewich, and T. F. Heinz, Physical Review Letters **101** (2008).
[14] T. Mueller, F. N. A. Xia, and P. Avouris, Nature Photonics **4**, 297 (2010).
[15] L. Yang, J. Deslippe, C. H. Park, M. L. Cohen, and S. G. Louie, Physical Review Letters **103** (2009).
[16] L. C. Campos, V. R. Manfrinato, J. D. Sanchez-Yamagishi, J. Kong, and P. Jarillo-Herrero, Nano Letters **9**, 2600 (2009).
[17] J. S. Bunch, Y. Yaish, M. Brink, K. Bolotin, and P. L.

McEuen, Nano Letters **5**, 287 (2005).
[18] T. Ihn, S. Gustavsson, U. Gasser, B. Kung, T. Muller, R. Schleser, M. Sigrist, I. Shorubalko, R. Leturcq, and K. Ensslin, Solid State Communications **149**, 1419 (2009).
[19] L. A. Ponomarenko, F. Schedin, M. I. Katsnelson, R. Yang, E. W. Hill, K. S. Novoselov, and A. K. Geim, Science **320**, 356 (2008).
[20] B. Wunsch, T. Stauber, and F. Guinea, Phys. Rev. B **77** , 035316 (2008).
[21] J. Wurm, A. Rycerz, I. Adagideli, M. Wimmer, K. Richter, and H. U. Baranger, Phys. Rev. Lett. **102** , 056806 (2009).
[22] F. Libisch, C. Stampfer, and J. Burgdorfer, Phys. Rev. B **79** , 115423 (2009).
[23] J. Akola, H. P. Heiskanen, and M. Manninen, Phys. Rev. B **77** , 193410 (2008).
[24] M. Ezawa, Phys. Rev. B **81** , 201402 (2010).
[25] P. Potasz, A. D. Güçlü, and P. Hawrylak, Physical Review B **81** (2010).
[26] A. D. Güçlü, P. Potasz, O. Voznyy, M. Korkusinski, and P. Hawrylak, Physical Review Letters **103** (2009).
[27] M. Ezawa, Phys. Rev. B **76** , 245415 (2007).
[28] J. Fernandez-Rossier and J. J. Palacios, Phys. Rev. Lett. **99** , 177204 (2007).
[29] W. L. Wang, S. Meng, and E. Kaxiras, Nano Letters **8**, 241 (2008).
[30] T. Yamamoto, T. Noguchi, and K. Watanabe, Physical Review B **74** (2006).
[31] Z. Z. Zhang, K. Chang, and F. M. Peeters, Phys. Rev. B **77**, 235411 (2008).
[32] X. Yan, X. Cui, B. S. Li, and L. S. Li, Nano Letters **10**, 1869 (2010).
[33] K. A. Ritter and J. W. Lyding, Nature Materials **8**, 235 (2009).
[34] D. K. Armani, T. J. Kippenberg, S. M. Spillane, and K. J. Vahala, Nature **421**, 925 (2003).
[35] A. Luque and A. Marti, Advanced Materials **22**, 160 (2010).
[36] P. Hawrylak, M. Korkusinski, Topics in Applied Physics **90** , 25-92 (Springer-Verlag 1985).